

Exotic Bohmian arrival times of spin-1/2 particles: An analytical treatmentSiddhant Das,^{*} Markus Nöth,[†] and Detlef Dürr[‡]*Mathematisches Institut, Ludwig-Maximilians-Universität München, Theresienstr. 39, D-80333 München, Germany*

(Received 25 January 2019; published 28 May 2019)

It is well known that orthodox quantum mechanics does not make unambiguous predictions for the statistics in arrival time (or time-of-flight) experiments. Bohmian mechanics (or de Broglie–Bohm theory) offers a distinct conceptual advantage in this regard, owing to the well-defined concepts of point particles and trajectories embedded in this theory. We revisit a recently proposed experiment [S. Das and D. Dürr, *Sci. Rep.* **9**, 2242 (2019)], the numerical analysis of which revealed a striking spin dependence in the (Bohmian) time-of-arrival distributions of a spin-1/2 particle. We present here a mathematically tractable variant of the same experiment, where the predicted effects can be established rigorously. We also obtain some results that can be compared with experiment.

DOI: [10.1103/PhysRevA.99.052124](https://doi.org/10.1103/PhysRevA.99.052124)**I. INTRODUCTION**

The description of arrival times of a quantum particle at a detector (e.g., a scintillation screen in the double-slit experimental setup) is an unsettled issue. A very careful analysis of arrival times within the framework of standard quantum mechanics was initiated by Allcock [1,2], but did not find a definite arrival time distribution. Noteworthy in this regard is also the earlier work of Aharonov and Bohm [3]. For more recent reviews see [4,5] and ([6], Chap. 5). It is also known that time is not a quantum observable in the canonical sense of a self-adjoint operator, hence there is no clear (or unique) way to address this problem from first principles of orthodox quantum mechanics. In fact, many theoretical proposals for the arrival time distribution of a particle (claimed to be) based on orthodox quantum mechanics turn out to be *ambiguous*, and at times even paradoxical [7,8], not to mention only vaguely connected to experiments [9]. It is also known that the statistics of standard quantum measurements are given by positive operator valued measures (POVMs; also referred to as generalized observables) on the particle’s Hilbert space [10]. In principle, specifying the POVM associated with a given arrival time experiment requires a full quantum mechanical analysis of the macroscopic system comprised of the apparatus and the particle. Since this is practically impossible, there have been many attempts to guess a universal POVM or a universal class of POVMs from symmetry or other principles of orthodox quantum mechanics [3,11–14]. To our knowledge, none of the POVMs suggested have been experimentally verified in a serious manner.

We shall study in this paper the arrival time problem within the framework of Bohmian mechanics, which offers a broader viewpoint on quantum phenomena, not limited by self-adjoint operators or POVMs. More importantly, due to the well-defined concepts of point particles and trajectories

embedded in this theory, it is naturally suited for computing arrival times of a particle. The virtues of Bohmian trajectories in the context of tunneling times have been recognized in recent publications [15,16]. We focus on certain special wave functions that can be prepared (e.g., ground states of a potential), and for which the Bohmian arrival time distributions show very striking behavior. Indeed, the distributions we find are so extremely well articulated that their existence almost demands experimental inspection.

We refer to the Bohmian arrival time distributions as *ideal* or *intrinsic* distributions, since the influence of the detector is ignored in our theoretical treatment. Such an idealization proves to be satisfactory in many applications, e.g., the double-slit experiment, Fig. 1. See [17] for a weak measurement of average quantum trajectories in a double-slit experiment, which can indeed be seen as Bohmian trajectories. In a followup to this paper [18] we model the influence of a physical detector (via a phenomenological imaginary potential [2]), which supports our conviction that the ideal arrival time distributions are in fact good approximations to the measured ones.

So far, there exist no experimental data for arrival time distributions other than that obtained in the “far field” or scattering regime [20–25]. In such experiments, the scattered particle after leaving the source travels freely for a *long distance* (compared to the width of its wave function at the time of preparation), and the measured time of flight (TOF) of the particle is explained classically, tacitly assuming the validity of Newtonian mechanics. Such treatments are routinely used for fitting TOF data, both in single-particle experiments involving heavy ions (e.g., $^{40}\text{Ca}^+$, $^{90}\text{Th}^+$) [23,26] and many-body experiments [24,25] involving a cloud of $\approx 10^3$ atoms.

The empirical success of semiclassical methods is not altogether surprising from a Bohmian viewpoint, since the emergence of Newtonian behavior in scattering situations is an ubiquitous feature of this theory. In particular, the wave function of a particle in far field (potential-free) regions becomes an approximate plane wave; consequently the Bohmian trajectories become nearly straight lines of *constant* velocity, similar to the Newtonian trajectories of a free particle. On

^{*}Siddhant.Das@physik.uni-muenchen.de[†]noeth@math.lmu.de[‡]duerr@mathematik.uni-muenchen.de

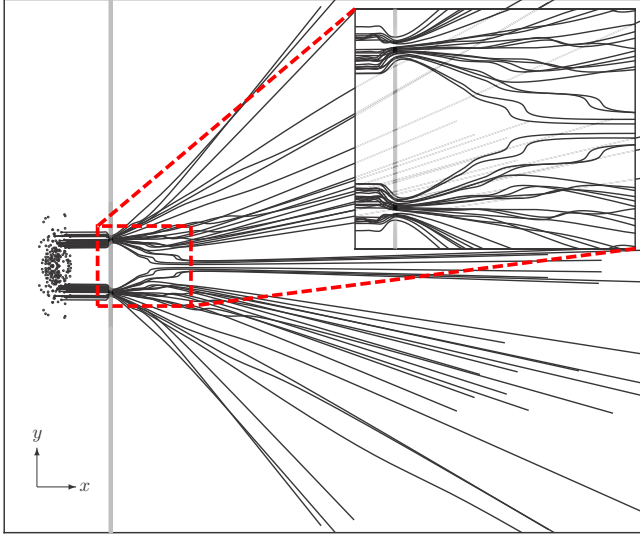


FIG. 1. Collection of Bohmian trajectories of a spin-0 particle passing through a double-slit interferometer, with initial positions sampled randomly from the initial $|\psi|^2$ distribution (dots). Most trajectories are reflected back (not shown). Inset: magnified view of the near field region. Figure courtesy of Kellers [19].

the contrary, in the near field (e.g., close to the slits in a double-slit setup, Fig. 1), the particle is influenced by interference of wave packets, causing its trajectory to meander in a non-Newtonian manner. The (Bohmian) arrival time of the particle at a *distant screen* is thus to a good approximation explained by classical reasoning, ignoring the negligible time spent in the near field region. Therefore, soliciting deviations from semiclassical methods, theorists (including those approaching the problem from non-Bohmian viewpoints) have recommended “moving the detectors closer to the region of coherent wave packet production, or closer to the interaction region” ([5], p. 419). However, such a relocation may not only disturb the wave function of the particle in an undesirable way [27], but also require cutting edge time resolution equipment.

Based on these considerations, an arrival time experiment for a spin-1/2 particle was proposed in [28,29], which had the distinctive virtue that the particle in the course of its flight *never* moved freely. Therefore, the Bohmian arrival time was not given by a classical formula (as in the far field scattering situations discussed above). Most importantly, in this experiment the nonclassical motion was *not* caused by the interference of waves (as in the regions close to the slits), but was instead due to the *spin term* found in the Bohmian guidance law of a spin-1/2 particle (explained below). The obtained arrival time distributions revealed a remarkable spin dependence, hitherto unknown. Furthermore, all distinguishing features were well preserved even with the detector placed at large distances from the source; hence the predictions could be checked by present-day experiments.

II. RECAP OF THE EXPERIMENT PROPOSED IN [28]

A spin-1/2 particle of mass m is constrained to move in a long waveguide, modeled as a semi-infinite cylinder. Initially, it is trapped between the end face of the waveguide and an

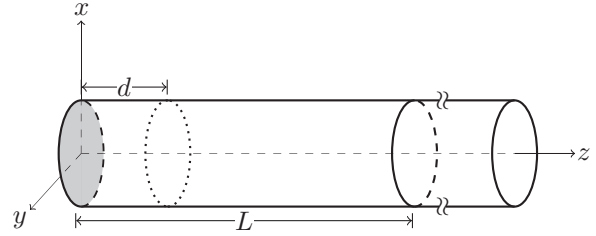


FIG. 2. Schematic drawing of the experimental setup. The barrier at d is switched off at $t = 0$ and arrival times are monitored at $z = L$.

impenetrable potential barrier placed at a distance d , as shown in Fig. 2. At the start of the experiment, the particle is prepared in a ground state Ψ_0 of this cylindrical box; then the barrier at d is suddenly switched off, say, $t = 0$, allowing the particle to propagate freely within the waveguide. A suitable detector records the arrival time (or TOF) τ of the particle on the *plane* situated a distance $L (> d)$ from the end face of the waveguide. We ask what is the distribution $\Pi^{\Psi_0}(\tau)$ of these arrival times?

In [28,29], the cylindrical confinement of the waveguide was modeled by a harmonic potential

$$V_{\perp}(x, y) = \frac{1}{2}m\omega^2(x^2 + y^2), \quad (1)$$

after popular quadrupole ion traps (also known as Paul traps), while the end face of the waveguide (i.e., the xy plane) and the barrier at d were modeled as hard-wall potential barriers. The ground-state wave functions of a spin-1/2 particle confined in such a cylindrical box have the form $\Psi_0(\mathbf{r}) = \psi_0(\mathbf{r})\chi$, where

$$\psi_0(\mathbf{r}) = \sqrt{\frac{2m\omega}{\pi\hbar d}} \theta(z)\theta(d-z) \sin(\pi z/d) e^{-\frac{m\omega}{2\hbar}(x^2+y^2)} \quad (2)$$

is the “spatial part” of the wave function, χ is a normalized two-component spinor ($\chi^\dagger\chi = 1$), and $\theta(\cdot)$ is Heaviside’s step function.

The instant the barrier is switched off, the wave function spreads dispersively, filling the volume of the waveguide. The particle moves along a definite Bohmian trajectory $\mathbf{R}(t) = X(t)\hat{\mathbf{x}} + Y(t)\hat{\mathbf{y}} + Z(t)\hat{\mathbf{z}}$ in accordance with Bohm’s *guidance law*, Eq. (6), below. For such an experimental setup, the *first* arrival time (or hitting time) of a trajectory starting at $\mathbf{R}_0 \equiv \mathbf{R}(0)$ and arriving at $z = L$ is

$$\tau(\mathbf{R}_0) = \min\{t | Z(t, \mathbf{R}_0) = L, \mathbf{R}_0 \in \text{supp}(\Psi_0)\}, \quad (3)$$

where $Z(t, \mathbf{R}_0) \equiv Z(t)$ is the z coordinate of the particle at time t and $\text{supp}(\Psi_0)$ denotes the support of the initial ground-state wave function (the region $0 < z < d$). The arrival time is thus a function of L and the initial position \mathbf{R}_0 . The initial positions realized in a sequence of experimental runs are random, with distribution given by $|\Psi_0|^2$ (see Sec. III); hence the density of the arrival time distribution

$$\Pi_{\text{Bohm}}^{\Psi_0}(\tau) = \int_{\text{supp}(\Psi_0)} d^3\mathbf{R}_0 \delta(\tau(\mathbf{R}_0) - \tau) |\Psi_0|^2(\mathbf{R}_0). \quad (4)$$

This distribution predicted an unexpected articulated feature for the so-called “up-down” ground-state wave function, characterized by

$$\chi = \frac{1}{\sqrt{2}} \begin{pmatrix} 1 \\ e^{i\beta} \end{pmatrix}, \quad 0 \leq \beta < 2\pi, \quad (5)$$

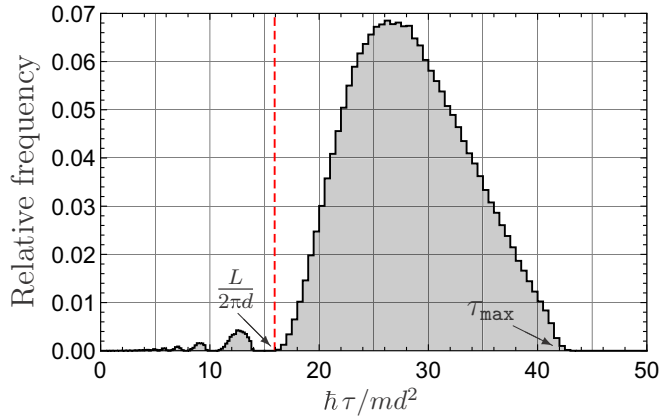


FIG. 3. Arrival time histogram $\Pi_{\text{Bohm}}^{\Psi_0}(\tau)$ versus (dimensionless) arrival time $\frac{\hbar\tau}{md^2}$ for the spin-up-down wave function: the detector is placed at $L = 100d$, and we have set $\beta = 0$ with $\omega = 10^3 \frac{\hbar}{md^2}$. The histogram was generated with 8×10^5 Bohmian trajectories whose initial points were randomly drawn from the Born $|\Psi_0|^2$ distribution. All Bohmian trajectories in this case strike the detector before $t = \tau_{\text{max}} \approx 42.9 \frac{md^2}{\hbar}$. An infinite train of self-similar smaller lobes, separated by distinct “no-arrival windows,” is seen below $\tau = 15.9 \frac{md^2}{\hbar}$ (dashed line).

namely, the density *vanished* beyond a characteristic arrival time $\tau = \tau_{\text{max}}$, which we called the “maximum arrival time” (see Fig. 3). That is, *all* Bohmian trajectories in this case strike the plane $z = L$ before $t = \tau_{\text{max}}$. Furthermore, the distributions for different choices of the parameter β turned out to be *identical* (a consequence of the cylindrical symmetry of the waveguide [30]) and displayed an infinite sequence of *self-similar* lobes below $\tau = \frac{mdL}{2\pi\hbar}$ (dashed line in Fig. 3), which diminished in size as $\tau \rightarrow 0$. It was also observed that the smaller lobes are separated by distinct gaps (or “no-arrival windows”) inside which the arrival time density is *zero*. Since the predicted distributions showed such interesting and significant behavior, we suggested that the proposed experiment be performed to test the predictive power of Bohmian mechanics for spin-1/2 particles.

The observations in [28], however, were based on numerical evidence, since analytical solutions for the trajectories were not available. In this paper we explain the emergence of the maximum arrival time with a mathematically tractable variant of the same experiment. The only modification is the replacement of the hard-wall potential barrier at $z = d$ by a smooth harmonic barrier $\frac{1}{2}m\omega_z^2 z^2$, which effectively limits the initial wave function to the region $0 < z < \sqrt{\hbar/m\omega_z}$, and which is switched off at $t = 0$. In this model, the time evolution of the wave function is greatly simplified, and we are able to prove rigorously that the drop-off in the up-down arrival time distribution manifests at a sharply defined time τ_{max} . This supports our conjecture that the notable features reported in [28] are generic and stable against perturbations.

We begin in Sec. III with a brief overview of the Bohmian mechanics of a spin-1/2 particle, applying it in Sec. IV to an analysis of the arrival time experiment. Focusing on two specific wave functions, viz., those of the spin-up (Ψ_{\uparrow}) and the spin-up-down (Ψ_{\downarrow}) ground states, we analyze the Bohmian

trajectories of the particle following its sudden release from the trap at $t = 0$. Arrival time distributions for these cases are found in Sec. V, where we also consider their behavior in the limit $\omega \rightarrow \infty$ (i.e., as the diameter of the waveguide goes to zero), keeping L fixed. The spin-up arrival time distribution (being *independent* of ω) remains unaffected, while the up-down arrival time distribution approaches a limiting distribution with $\tau_{\text{max}} \rightarrow \omega_z^{-1} \sqrt{(m\omega_z/\hbar)L^2 - 1}$. In Sec. VC we obtain an analytical formula for this limiting distribution, relegating most of the details to the mathematical Appendixes. On the other hand, both distributions *coincide* in the “no waveguide” limit, $\omega \rightarrow 0$. A confining waveguide is therefore essential to observing this intriguing spin dependence of the arrival time distributions. Section VI offers a general discussion and concludes with a heuristic explanation of the “no-arrival windows” found in Fig. 3.

III. ELEMENTS OF BOHMIAN MECHANICS

Bohm’s theory, like Newtonian mechanics, describes the motion of point particles. However, this dynamics is of first order; therefore, the motion of an *isolated* particle is governed by an equation of the type

$$\frac{d}{dt}\mathbf{R}(t) = \mathbf{v}_{\text{Bohm}}(\mathbf{R}(t), t), \quad (6)$$

where $\mathbf{R}(t) \in \mathbb{R}^3$ is the position of the particle at time t and \mathbf{v}_{Bohm} is the velocity field. In other words, Bohmian trajectories are integral curves of this (Bohmian) velocity field, i.e., a solution of Eq. (6) for some initial position $\mathbf{R}_0 \equiv \mathbf{R}(0)$.

The Bohmian velocity field for a spin-1/2 particle of mass m is given by [31,32, Chap. 10]

$$\mathbf{v}_{\text{Bohm}}(\mathbf{r}, t) = \frac{\hbar}{m} \text{Im} \left[\frac{\Psi^\dagger \nabla \Psi}{\Psi^\dagger \Psi} \right] + \frac{\hbar}{2m} \left[\frac{\nabla \times (\Psi^\dagger \boldsymbol{\sigma} \Psi)}{\Psi^\dagger \Psi} \right], \quad (7)$$

where $\Psi \equiv \Psi(\mathbf{r}, t)$, the wave function, is a two-component complex-valued spinor solution of the Pauli equation

$$i\hbar \frac{\partial}{\partial t} \Psi(\mathbf{r}, t) = -\frac{\hbar^2}{2m} (\boldsymbol{\sigma} \cdot \nabla)^2 \Psi(\mathbf{r}, t) + V(\mathbf{r}, t) \Psi(\mathbf{r}, t), \quad (8)$$

with given initial condition $\Psi_0(\mathbf{r})$, Ψ^\dagger is its adjoint, and $\boldsymbol{\sigma} = \sigma_x \hat{x} + \sigma_y \hat{y} + \sigma_z \hat{z}$ is a three-vector of Pauli spin matrices. Here, $V(\mathbf{r}, t)$ denotes an external potential characterizing the interactions of the particle with its surroundings. If magnetic fields are present, the gradient in Eqs. (7) and (8) should be understood as the gauge covariant derivative, involving the vector potential.

For almost every \mathbf{R}_0 (with respect to the $|\Psi_0|^2$ measure) and under general conditions on the initial wave function Ψ_0 and the potential V one has *existence* and *uniqueness* of Bohmian trajectories [33,34]. In particular, this implies that Bohmian trajectories *cannot* run into nodes (or zeros) of the wave function, where the velocity field is ill defined.

The dynamical equations (6), (7), and (8) are all time-reversal¹ and Galilean invariant. Moreover, Eqs. (6) and (7)

¹Unlike a scalar wave function, the time reversal transformation of a spinor is implemented by $\Psi \rightarrow -i\sigma_y \Psi^*$ ([35], Eq. 4.4.65).

are the *unique* nonrelativistic limit of the guidance equation for a relativistic spin-1/2 particle, whose wave function satisfies the Dirac equation [31,36,37].

In Bohmian mechanics the primary role of the wave function is to determine the motion of the particle, while its statistical significance is a derived consequence. As much as in Newtonian mechanics, unique initial conditions lead to unique outcomes via Eqs. (6) and (8); nevertheless, experimental predictions made by Bohmian mechanics are always probabilistic in character. This is because the initial particle positions realized in a sequence of identically prepared experiments (i.e., experiments with the same initial wave function Ψ_0) are typically random, with distribution given by $|\Psi_0|^2$ (see [38] for a justification). By virtue of the velocity field (7), the position of a Bohmian particle remains $|\Psi|^2$ distributed at *any* later time t . This property is known as *equivariance*.

The ostensible randomness, together with the equivariance of the $|\Psi|^2$ measure and its precise interpretation, imply that Bohmian predictions must agree with the predictions of orthodox quantum mechanics, whenever the latter are unambiguous (e.g., position, momentum, and spin measurements) [10,32]. As explained in the Introduction, there is no consensus on a quantum-mechanical prediction for the arrival time statistics of a particle at present. Thus our analysis provides a possibility to test the predictive power of a pragmatic application of Bohmian mechanics to arrival time experiments.

IV. FORMULATION

In Cartesian coordinates $\mathbf{r} = (x, y, z)$ the cylindrical waveguide depicted in Fig. 2 can be modeled by the potential

$$V(\mathbf{r}, t) = V_{\perp}(x, y) + V_{\parallel}(z, t), \quad (9)$$

where $V_{\perp}(x, y) = \frac{1}{2}m\omega^2(x^2 + y^2)$, as in (1), but the axial potential $V_{\parallel}(z, t) = v(z) + \theta(-t)\frac{1}{2}m\omega_z^2z^2$ is now comprised of a harmonic potential barrier (which is switched off at $t = 0$) and a hard-wall potential,

$$v(z) = \begin{cases} \infty, & z \leq 0, \\ 0, & z > 0, \end{cases} \quad (10)$$

delineating the end face of the waveguide. As the units of measurement of mass, length, and time we take, respectively,

$$m, \quad \sqrt{\hbar/m\omega_z}, \quad \text{and} \quad 1/\omega_z$$

(formally, this amounts to setting $\hbar = m = \omega_z = 1$ in all equations). From here on we will work in these units unless otherwise stated.

The ground-state wave function of a spin-1/2 particle confined in the trap (for $t < 0$) takes the general parametric form

$$\Psi_0(\mathbf{r}) = \psi_0(\mathbf{r}) \begin{pmatrix} \cos(\alpha/2) \\ \sin(\alpha/2)e^{i\beta} \end{pmatrix}, \quad \begin{matrix} 0 \leq \alpha \leq \pi, \\ 0 \leq \beta < 2\pi, \end{matrix} \quad (11)$$

where

$$\psi_0(\mathbf{r}) = A \theta(z) z e^{-\frac{z}{2} - \frac{\omega}{2}(x^2 + y^2)}, \quad (12)$$

One can easily verify that under this transformation \mathbf{v}_{Bohm} flips its direction.

and $A = \sqrt{4\omega/\pi}^{3/4}$ is a normalization constant. For the present discussion of arrival times we focus on two specific wave functions, viz.,

$$\Psi_{\uparrow}(\mathbf{r}, 0) = \psi_0(\mathbf{r}) \begin{pmatrix} 1 \\ 0 \end{pmatrix}, \quad \Psi_{\downarrow}(\mathbf{r}, 0) = \frac{\psi_0(\mathbf{r})}{\sqrt{2}} \begin{pmatrix} 1 \\ 1 \end{pmatrix}, \quad (13)$$

which correspond, respectively, to the choices $\alpha = \beta = 0$, and $\alpha = \frac{\pi}{2}, \beta = 0$, in (11), and will be referred to as the spin-up, and spin-up-down, wave functions, respectively. Here, up and up-down refers to the orientation of the “spin vector”

$$\mathbf{s} := \frac{1}{2} \frac{\Psi^{\dagger} \boldsymbol{\sigma} \Psi}{|\Psi|^2} = \frac{1}{2} \begin{cases} \hat{\mathbf{z}}, & \Psi = \Psi_{\uparrow}, \\ \hat{\mathbf{x}}, & \Psi = \Psi_{\downarrow}, \end{cases} \quad (14)$$

associated with the wave function Ψ , which is aligned parallel (perpendicular) to the waveguide axis in the case of Ψ_{\uparrow} (Ψ_{\downarrow}). Arrival time distributions for general α and β are discussed in [28–30].

The solutions of the Pauli equation, Eq. (8), with initial conditions (13), are (see Appendix A for details)

$$\Psi_{\uparrow}(\mathbf{r}, t) = \psi_t(\mathbf{r}) \begin{pmatrix} 1 \\ 0 \end{pmatrix}, \quad \Psi_{\downarrow}(\mathbf{r}, t) = \frac{\psi_t(\mathbf{r})}{\sqrt{2}} \begin{pmatrix} 1 \\ 1 \end{pmatrix}, \quad (15)$$

where

$$\psi_t(\mathbf{r}) = A \theta(z) \frac{z}{(1 + it)^{3/2}} \times \exp \left[-\frac{z^2}{2(1 + it)} - \frac{\omega}{2}(x^2 + y^2 + 2it) \right]. \quad (16)$$

We see that both wave functions propagate dispersively, filling the volume of the waveguide. Their axial widths $^2 \Delta_z(t) \approx 0.47\sqrt{1 + t^2}$ increase with time, while the transverse waveguide potential $V_{\perp}(x, y)$ keeps the wave packets from spreading in the lateral directions. Note that both wave functions vanish at $z = 0$, respecting the (Dirichlet) boundary condition at the end face of the waveguide. Note as well that

$$|\Psi_{\uparrow}(\mathbf{r}, t)|^2 = |\Psi_{\downarrow}(\mathbf{r}, t)|^2 = \psi_t^* \psi_t. \quad (17)$$

Hence the statistical distributions of particle *positions* within the waveguide are identical in both cases at any time t . However, this does not imply that the arrival time distributions should be identical, since these depend exclusively on the underlying dynamics encoded in the guidance law.

We turn now to the Bohmian trajectories, i.e., the solutions of Eq. (6). The first summand on the right-hand side of the Bohmian velocity field (7), the so-called *convective* velocity, is the same for both wave functions, viz.,

$$\text{Im} \left[\frac{\Psi^{\dagger} \nabla \Psi}{\Psi^{\dagger} \Psi} \right] = \frac{t z}{1 + t^2} \hat{\mathbf{z}}, \quad (18)$$

and is directed parallel to the axis of the waveguide. Similarly, the second summand (also known as the *spin* velocity) can be calculated explicitly. Since $\nabla \times \mathbf{s} = 0$ in both cases [cf. Eq. (14)], the spin velocity can be written as

$$\frac{\nabla \times (\Psi^{\dagger} \boldsymbol{\sigma} \Psi)}{2 \Psi^{\dagger} \Psi} = \nabla (\ln |\psi_t|^2) \times \mathbf{s}$$

$^2 \Delta_z(t) := \sqrt{\langle z^2 \rangle_{\Psi} - \langle z \rangle_{\Psi}^2}$.

$$= \begin{cases} -\omega(y\hat{x} - x\hat{y}), & \Psi = \Psi_{\uparrow}, \\ \left(\frac{1}{z} - \frac{z}{1+t^2}\right)\hat{y} + \omega y\hat{z}, & \Psi = \Psi_{\downarrow}. \end{cases} \quad (19)$$

The particle position at time t is $\mathbf{R}(t) = X(t)\hat{x} + Y(t)\hat{y} + Z(t)\hat{z}$. Its time derivative $\dot{\mathbf{R}}(t)$ features in the guidance equation (6), the right-hand side of which can be evaluated using Eqs. (18) and (19) to obtain the component equations

$$\dot{X} = -\omega Y, \quad (20a)$$

$$\dot{Y} = \omega X, \quad (20b)$$

$$\dot{Z} = \frac{t}{1+t^2}Z, \quad (20c)$$

for the spin-up wave function, and

$$\dot{X} = 0, \quad (21a)$$

$$\dot{Y} = \frac{1}{Z} - \frac{Z}{1+t^2}, \quad (21b)$$

$$\dot{Z} = \omega Y + \frac{t}{1+t^2}Z, \quad (21c)$$

for the spin-up-down wave function.

In view of Eqs. (20) and (21), the reader might be concerned that the wave function symmetry in the x and y coordinates has been lost in the guidance equations. However, this should come as no surprise, since the spin vector \mathbf{s} picks out a preferred direction in each case. We proceed next to the solution of these coupled ODEs with initial condition $\mathbf{R}_0 = X_0\hat{x} + Y_0\hat{y} + Z_0\hat{z}$.

A. Bohmian trajectories for Ψ_{\uparrow}

The differential equation for the z coordinate, Eq. (20c), is separable and admits a simple solution:

$$Z(t) = Z_0\sqrt{1+t^2}. \quad (22)$$

Moving now to Eqs. (20a) and (20b), an easy way of solving these is to introduce a complex coordinate

$$S(t) := X(t) + iY(t), \quad (23)$$

the time derivative of which is

$$\dot{S} = \dot{X} + i\dot{Y} = \omega(-Y + iX) = i\omega S. \quad (24)$$

Equation (24) is readily solved:

$$S(t) = S_0 e^{i\omega t}, \quad S_0 = X_0 + iY_0, \quad (25)$$

and the desired solutions can be read off from the real and imaginary parts of Eq. (25), viz.,

$$X(t) = X_0 \cos(\omega t) - Y_0 \sin(\omega t), \quad (26a)$$

$$Y(t) = Y_0 \cos(\omega t) + X_0 \sin(\omega t). \quad (26b)$$

From Eq. (25) we also see that $|S(t)|^2 = X^2(t) + Y^2(t) = |S_0|^2$ is a constant of motion. The angular velocity of the particle about the z axis, given by

$$\frac{d}{dt} \text{Arg}[S(t)] = \omega,$$

is a constant as well. Therefore, a spin-up Bohmian trajectory is a circular *helix* of radius $|S_0|$, which circulates in an anti-

clockwise sense about the waveguide axis (see Table I for an example).

B. Bohmian trajectories for Ψ_{\downarrow}

The first equation, Eq. (21a), has the obvious solution

$$X(t) = X_0, \quad (27)$$

the initial value of X . Consider next Eqs. (21b) and (21c): these equations are also analytically integrable; however, the solutions can only be written in terms of certain nontrivial integrals (i.e., solution by quadrature). Introducing a new function ξ defined by

$$Z(t) = \xi(t)\sqrt{1+t^2}, \quad (28)$$

Eqs. (21b) and (21c) can be written as

$$\dot{Y} = \frac{1}{\sqrt{1+t^2}} \left(\frac{1}{\xi} - \xi \right), \quad (29a)$$

$$\dot{\xi} = \frac{\omega}{\sqrt{1+t^2}} Y. \quad (29b)$$

Dividing Eq. (29a) by Eq. (29b), we find

$$\begin{aligned} \frac{d}{dt} \left[\ln |\xi(t)| - \frac{1}{2} \xi^2(t) - \frac{\omega}{2} Y^2(t) \right] &= 0, \\ \Rightarrow \ln \xi^2(t) - \xi^2(t) - \omega Y^2(t) &= \text{const}, \end{aligned} \quad (30)$$

an extremely useful constant of motion. Since Eq. (30) holds for all t on the trajectory, one can fix the constant of integration from the initial conditions, i.e.,

$$\begin{aligned} \ln \xi^2(t) - \xi^2(t) - \omega Y^2(t) &= \ln Z_0^2 - Z_0^2 - \omega Y_0^2 \\ &=: \ln(-g), \end{aligned} \quad (31)$$

noting $\xi(0) = Z_0$ from Eq. (28). We have introduced

$$g = -Z_0^2 e^{-Z_0^2 - \omega Y_0^2} \equiv g(Y_0, Z_0) \quad (32)$$

for brevity. Solving for Y in (31), we obtain

$$Y(t) = \pm \sqrt{\frac{\ln(\xi^2(t)/-g) - \xi^2(t)}{\omega}}. \quad (33)$$

Substitution of (33) in (29b) then yields

$$\text{sgn}(Y) \frac{d\xi}{\sqrt{\ln(\xi^2/-g) - \xi^2}} = \sqrt{\omega} \frac{dt}{\sqrt{1+t^2}}, \quad (34)$$

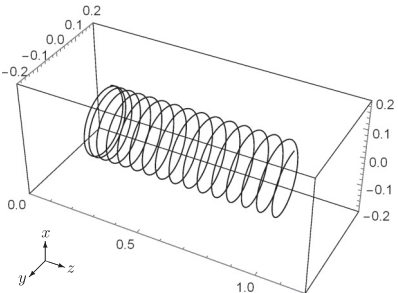
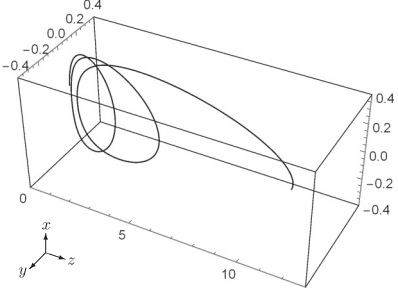
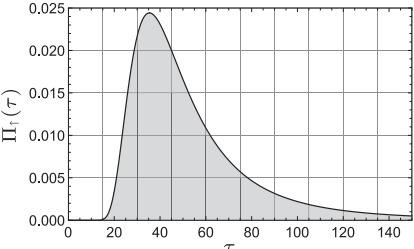
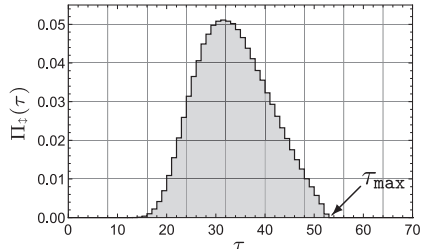
where $\text{sgn}(\cdot)$ is the signum function. In order to integrate the above, we characterize the variation of $\text{sgn}(Y)$ with respect to ξ as follows: observe that $\xi(t)$ attains an *extremum* (either a maximum or a minimum) whenever $Y = 0$ [cf. Eq. (29b)]. These extreme values, $\bar{\xi}$, therefore satisfy

$$\begin{aligned} \ln(\bar{\xi}^2/-g) - \bar{\xi}^2 &= 0 \Rightarrow -\bar{\xi}^2 e^{-\bar{\xi}^2} = g \\ &\Rightarrow -\bar{\xi}^2 = W(g) \\ &\Rightarrow \bar{\xi} = \pm \sqrt{-W(g)}, \end{aligned} \quad (35)$$

where $W(\cdot)$ is the Lambert W function (or product logarithm) [39]. For the values of g permitted by the initial conditions [Eq. (32)], viz.,

$$-1/e \leq g < 0, \quad (36)$$

TABLE I. Overview of results and essential details of the paper. Here, ${}_1F_1(a; b; z)$ denotes the confluent hypergeometric function of the first kind.

Wave function:	$\Psi_{\uparrow}(\mathbf{r}, t) = \psi_{\uparrow}(\mathbf{r}) \binom{1}{0}$	$\Psi_{\downarrow}(\mathbf{r}, t) = \frac{\psi_{\downarrow}(\mathbf{r})}{\sqrt{2}} \binom{1}{1}$
Position probability density: $\Psi^{\dagger}\Psi$	$ \psi_{\uparrow}(\mathbf{r}) ^2$	$ \psi_{\downarrow}(\mathbf{r}) ^2$
Spin vector: $\mathbf{s} = \frac{1}{2} \frac{\Psi^{\dagger}\boldsymbol{\sigma}\Psi}{\Psi^{\dagger}\Psi}$	$\frac{1}{2} \hat{\mathbf{z}}$ (along waveguide axis)	$\frac{1}{2} \hat{\mathbf{x}}$ (perpendicular to waveguide axis)
Guiding equations	$\begin{aligned} \dot{X} &= -\omega Y \\ \dot{Y} &= \omega X \\ \dot{Z} &= \frac{t}{1+t^2} Z \end{aligned}$	$\begin{aligned} \dot{X} &= 0 \\ \dot{Y} &= \frac{1}{2} - \frac{Z}{1+t^2} \\ \dot{Z} &= \omega Y + \frac{t}{1+t^2} Z \end{aligned}$
Constants of motion	$X^2 + Y^2$ and $X\dot{Y} - Y\dot{X}$	$\ln\left(\frac{Z^2}{1+t^2}\right) - \frac{Z^2}{1+t^2} - \omega Y^2$ and X
Typical Bohmian trajectories for respective wave functions: $\mathbf{R}(0) = 0.05\hat{\mathbf{x}} + 0.1\hat{\mathbf{y}} + 0.2\hat{\mathbf{z}}$ and $\omega = 20$; both trajectories are plotted for the time interval $[0, 2]$		
Arrival time distributions for $L = 50$ and $\omega = 500$		
Distribution function	$\Pi_{\uparrow}(\tau) = \frac{4L^3}{\lambda_0\sqrt{\pi}} \frac{\tau e^{-\frac{L^2}{1+\tau^2}}}{(1+\tau^2)^{5/2}}$	No closed form expression for $\Pi_{\downarrow}(\tau)$
Behavior for large τ	Heavy tailed $\sim \frac{4L^3}{\lambda_0\sqrt{\pi}} \tau^{-4} + O(\tau^{-6})$, as $\tau \rightarrow \infty$	Vanishes for all $\tau > \tau_{\max}$
Behavior for small ω	Independent of ω	Reduces to $\Pi_{\uparrow}(\tau)$, as $\omega \rightarrow 0$, while $\tau_{\max} \rightarrow \infty$
Behavior for large ω	Independent of ω	Convergence to $\Pi_{\downarrow}(\tau)$, as $\omega \rightarrow \infty$, while $\tau_{\max} \rightarrow \sqrt{L^2 - 1}$
Arrival time moments	$\langle \tau^{\mu} \rangle_{\uparrow} = \frac{4L^3}{3\lambda_0\sqrt{\pi}} \begin{cases} {}_1F_1(1; \frac{3}{2}; -L^2), & \mu = 1 \\ {}_2F_1(\frac{1}{2}; \frac{5}{2}; -L^2), & \mu = 2 \\ \infty, & \mu > 2 \end{cases}$	All moments are finite

there are two possible real values of $W(g)$ (see Fig. 4), denoted by $W_{-1}(g)$ and $W_0(g)$. Since $\xi(t) > 0$,³ we discard the negative radical in Eq. (35). Thus

$$\xi_s := \sqrt{-W_0(g)}, \quad \xi_b := \sqrt{-W_{-1}(g)}, \quad (37)$$

satisfying $\xi_s \leq \xi_b$ are the *only* possible extreme values of $\xi(t)$. The following inequality must therefore hold at any given

³The “node evading” property of Bohmian trajectories discussed in Sec. III implies that the trajectories do not penetrate the base of the waveguide (the xy plane), which is a stationary node of Ψ_{\downarrow} . Therefore, $Z(t)$ (consequently, $\xi(t) = Z(t)/\sqrt{1+t^2} > 0$ for all t .

time t :

$$\xi_s \leq \xi(t) \leq \xi_b. \quad (38)$$

A schematic plot of $\xi(t)$ is depicted in Fig. 5.

Since $Y(t)$ changes sign whenever $\xi(t)$ attains an extremum ($Y \propto \dot{\xi}$), integrating Eq. (34) between $t = 0$ and some generic time t for the example shown in Fig. 5 yields

$$\begin{aligned} & \int_{z_0}^{\xi_b} \frac{d\xi}{\sqrt{\ln(\xi^2/g) - \xi^2}} - \int_{\xi_b}^{\xi_s} \frac{d\xi}{\sqrt{\dots}} + \int_{\xi_s}^{\xi_b} \frac{d\xi}{\sqrt{\dots}} \\ & - \int_{\xi_b}^{\xi(t)} \frac{d\xi}{\sqrt{\dots}} = \int_{z_0}^{\xi_b} \frac{d\xi}{\sqrt{\dots}} + 2 \int_{\xi_s}^{\xi_b} \frac{d\xi}{\sqrt{\dots}} - \int_{\xi_b}^{\xi(t)} \frac{d\xi}{\sqrt{\dots}} \\ & = \sqrt{\omega} \sinh^{-1} t, \end{aligned} \quad (39)$$

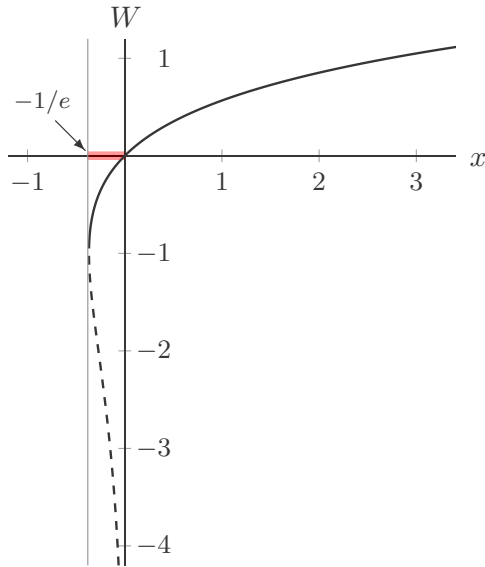


FIG. 4. Two real branches of $W(x)$: $W_{-1}(x)$ (dashed); $W_0(x)$ (solid). The thick red line emphasizes the interval $[-1/e, 0]$, the range of the function $g(Y_0, Z_0)$.

where we omitted writing the radical explicitly in the integrals above for brevity. Note that a general trajectory attains ξ_b as the first extremum only if $Y_0 > 0$ (as in Fig. 5); otherwise it attains ξ_s . Consequently, the lower limit of the last integral changes depending on the number of half-cycles n that are completed between $t = 0$ and time t . If n is even [e.g., 2, as in Eq. (39)], the lower limit of integration of the last term equals the upper limit of integration of the first term. If n is odd, these limits are different. The generalization of Eq. (39) for any trajectory may be written as

$$\int_{Z_0}^{\xi_b} \frac{d\xi}{\sqrt{\ln(\xi^2/g) - \xi^2}} + n \int_{\xi_s}^{\xi_b} \frac{d\xi}{\sqrt{\dots}} + (-1)^{n+1} \times \int_{\frac{\xi_b + \xi_s}{2} + (-1)^n \frac{\xi_b - \xi_s}{2}}^{\xi(t)} \frac{d\xi}{\sqrt{\dots}} = \sqrt{\omega} \sinh^{-1} t \quad (Y_0 > 0), \quad (40a)$$

$$- \int_{Z_0}^{\xi_s} \frac{d\xi}{\sqrt{\ln(\xi^2/g) - \xi^2}} + n \int_{\xi_s}^{\xi_b} \frac{d\xi}{\sqrt{\dots}} + (-1)^n \times \int_{\frac{\xi_b + \xi_s}{2} - (-1)^n \frac{\xi_b - \xi_s}{2}}^{\xi(t)} \frac{d\xi}{\sqrt{\dots}} = \sqrt{\omega} \sinh^{-1} t \quad (Y_0 < 0), \quad (40b)$$

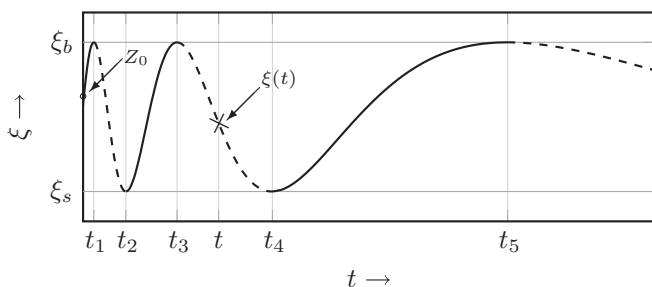


FIG. 5. Schematic plot of $\xi(t)$ against t , showing the extreme values ξ_s and ξ_b . Note that $\xi(0) = Z_0$ and $\dot{\xi}(t) = Y(t) = 0$ at the instants t_1, t_2, \dots, t_5 . The solid (dashed) parts of the curve correspond to $Y(t) > 0$ (< 0).

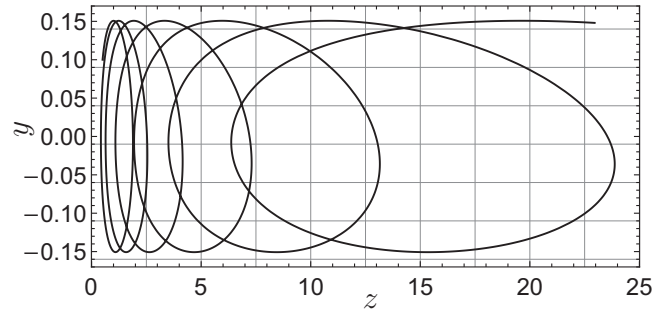


FIG. 6. Typical Bohmian trajectory of a spin-1/2 particle with wave function Ψ_{\uparrow} and initial position $\mathbf{R}_0 = 0.3\hat{x} + 0.1\hat{y} + 0.5\hat{z}$, the x coordinate of which is a constant of motion. The trajectory is plotted for the time interval $[0, 20]$ with $\omega = 50$.

where the slightly complicated expressions in the lower limits of each of the last integrals ensure the correct choice of ξ_b or ξ_s according to the rule explained above. Although Eq. (40) gives $\xi(t)$ only implicitly, it plays a crucial role in explaining the arrival time statistics of the up-down wave function. Once $\xi(t)$ is found, the complete trajectory of the particle is (implicitly) determined via Eqs. (28) and (33). A typical Bohmian trajectory is depicted in Fig. 6.

V. ARRIVAL TIME STATISTICS

The first arrival time (or passage time) of a trajectory starting at \mathbf{R}_0 and arriving at $z = L$ is given by Eq. (3), where $\text{supp}(\Psi_0)$, the support of the initial wave function, now denotes the half-space $z \geq 0$.⁴ Since the initial position is $|\Psi_0|^2$ distributed with $\Psi_0 \sim e^{-z^2/2}$, a few initial positions (those with $Z_0 > L$) will be realized behind the detector surface. Since $L \gg 1$, such spurious initial conditions are rare and can be discarded. We renormalize the arrival time distribution Eq. (4) accordingly:

$$\Pi_{\uparrow/\downarrow}(\tau) = \frac{\int_{0 < Z_0 < L} d^3\mathbf{R}_0 \delta(\tau(\mathbf{R}_0) - \tau) |\Psi_{\uparrow/\downarrow}(\mathbf{R}_0, 0)|^2}{\int_{0 < Z_0 < L} d^3\mathbf{R}_0 |\Psi_{\uparrow/\downarrow}(\mathbf{R}_0, 0)|^2}, \quad (41)$$

denoting the spin-up (spin-up-down) arrival time distribution as $\Pi_{\uparrow}(\tau)$ ($\Pi_{\downarrow}(\tau)$) for brevity. Here,

$$\tau(\mathbf{R}_0) = \min\{t \mid Z(t) = L, 0 < Z_0 < L\}. \quad (42)$$

Recalling that

$$|\Psi_{\uparrow/\downarrow}(\mathbf{R}_0, 0)|^2 = \frac{4\omega}{\pi^{3/2}} \theta(Z_0) Z_0^2 e^{-Z_0^2 - \omega(X_0^2 + Y_0^2)} \quad (43)$$

in both cases [cf. Eq. (13)], the denominator of Eq. (41) can be evaluated explicitly:

$$\int_{0 < Z_0 < L} d^3\mathbf{R}_0 |\Psi_{\uparrow/\downarrow}(\mathbf{R}_0, 0)|^2 = \text{erf}(L) - \frac{2L}{\sqrt{\pi}} e^{-L^2} \equiv \lambda_0, \quad (44)$$

⁴Compare this with the ground state (2) of [28], which was supported on the bounded region $0 \leq z \leq d$.

where $\text{erf}(\cdot)$ denotes the error function. In what follows, we consider the arrival time distributions on a case-by-case basis.

A. Arrival times for Ψ_\uparrow

The spin-up Bohmian trajectories propagate axially outward, each one crossing $z = L$ at most once. Using the exact solution for the trajectory, Eq. (22), the first arrival time (or simply the arrival time) is given by

$$\tau(\mathbf{R}_0) = \sqrt{(Z_0/L)^2 - 1}. \quad (45)$$

Since this depends only on Z_0 , the X_0 and Y_0 integrals in Eq. (41) can be readily evaluated, yielding

$$\Pi_\uparrow(\tau) = \frac{4}{\lambda_0 \sqrt{\pi}} \int_0^L dZ_0 \delta(\sqrt{(L/Z_0)^2 - 1} - \tau) Z_0^2 e^{-Z_0^2}. \quad (46)$$

In order to evaluate the above integral and for later use, we recall the identity

$$\delta(\phi(x)) = \sum_n \frac{\delta(x - x_n)}{|\phi'(x_n)|}, \quad (47)$$

where x_n is a zero of the function ϕ , ϕ' denotes its derivative, and the sum runs over all zeros of ϕ . For

$$\phi(Z_0) = \sqrt{(L/Z_0)^2 - 1} - \tau, \quad (48)$$

we obtain two zeros, viz.,

$$Z_{0\pm} = \pm \frac{L}{\sqrt{1 + \tau^2}}, \quad (49)$$

and evaluating the derivatives of ϕ at $Z_{0\pm}$, we have

$$\delta(\sqrt{(L/Z_0)^2 - 1} - \tau) = \frac{\tau Z_0^3}{L^2} [\delta(Z_0 - Z_{0+}) + \delta(Z_0 - Z_{0-})]. \quad (50)$$

Since $Z_{0-} < 0$, only the first delta function term contributes to the integral and we obtain

$$\Pi_\uparrow(\tau) = \frac{4L^3}{\lambda_0 \sqrt{\pi}} \frac{\tau e^{-\frac{L^2}{1+\tau^2}}}{(1 + \tau^2)^{5/2}}. \quad (51)$$

Figure 7 plots $\Pi_\uparrow(\tau)$ for different values of L . It follows from the above that

$$\Pi_\uparrow(\tau) \sim \frac{4L^3}{\lambda_0 \sqrt{\pi}} \tau^{-4} + O(\tau^{-6}), \quad (52)$$

as $\tau \rightarrow \infty$. This asymptotic behavior seems to be a characteristic feature of the spin-up distribution [28,30], and implies that only the mean first arrival time $\langle \tau \rangle_\uparrow$, and $\langle \tau^2 \rangle_\uparrow$ are finite (see Table I for exact formulas), while *all* higher moments diverge.

Note as well that $\Pi_\uparrow(\tau)$ is independent of the trapping frequency ω , which dropped out obligingly in Eq. (46). The reason is that the motion in the z direction decouples from the evolution of the x and y coordinates of the particle [cf. Eq. (20)]. The arrival time of any trajectory thus depends only on Z_0 . Furthermore, since the initial wave function Ψ_\uparrow is separated in the position coordinates, Z_0 is distributed independently with density $4Z_0^2 \theta(Z_0) \exp(-Z_0^2)/\sqrt{\pi}$, which is also independent of ω .

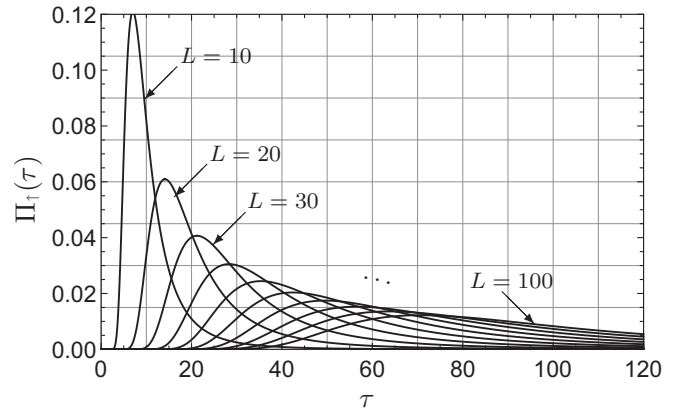


FIG. 7. Graphs of Π_\uparrow vs τ for select values of L . The distribution stretches over larger arrival times with increasing L .

B. Arrival times for Ψ_\downarrow

In this case an explicit formula for $\tau(\mathbf{R}_0)$, such as Eq. (45) cannot be found, as the Bohmian trajectories are known only implicitly (cf. Sec. IV B). Moreover, considering the quasiperiodic character of ξ (Fig. 5), a typical Bohmian trajectory intersects the plane $z = L$ multiple times, as shown in Fig. 8. Experimentally, of course, only the first crossing time $t_1 (= \tau)$ is relevant (the time at which the particle is detected). However, $Z(t_k) = L$ at *any* crossing time t_k , which as a result of Eq. (28) and inequality (38) implies

$$\xi_s \leq \frac{L}{\sqrt{1 + t_k^2}} \leq \xi_b. \quad (53)$$

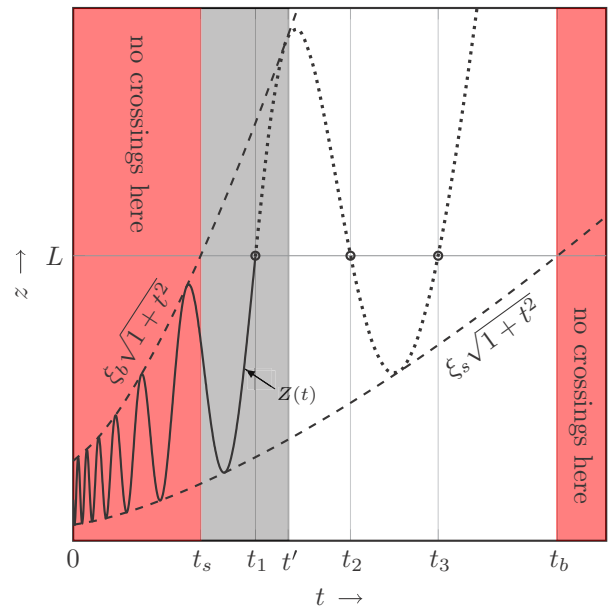


FIG. 8. Schematic plot of $Z(t)$ vs t for a spin-up-down Bohmian trajectory, enveloped between the dashed curves $\xi_s \sqrt{1 + t^2}$ and $\xi_b \sqrt{1 + t^2}$. The trajectory intersects $z = L$ at the instants $t_1 (= \tau)$, t_2 , and t_3 , which lie in the interval $[t_s, t_b]$, in accordance with (55). t' denotes the *first* instant after t_s at which the trajectory touches the upper envelope.

Solving for t_k above, keeping in mind that

$$0 < \xi_s \leq 1, \quad 1 \leq \xi_b < \infty \quad (54)$$

[cf. Eq. (37)], yields an analogous inequality for any crossing time of a Bohmian trajectory:

$$t_s \leq t_k \leq t_b, \quad (55)$$

where

$$t_s := \theta(L - \xi_b) \sqrt{\frac{L^2}{\xi_b^2} - 1}, \quad t_b := \sqrt{\frac{L^2}{\xi_s^2} - 1}. \quad (56)$$

That is, any crossing of a given trajectory, including the first one, commences before time t_b . However, recalling Eq. (32), one finds that g approaches zero whenever Y_0 or Z_0 become very large, or even when $Z_0 \approx 0$; consequently $\xi_s = \sqrt{-W_0(g)}$ also approaches zero (see Fig. 4). For such initial conditions, t_b gets arbitrarily large and hence does not explain the uniform upper bound on the arrival times (τ_{\max}) found in Fig. 3.

To derive such a bound, consider the *first* instant after $t = t_s$, say t' , at which a given trajectory touches the upper envelope $\xi_b \sqrt{1 + t'^2}$, depicted in Fig. 8. At this instant, $Z(t') = \xi_b \sqrt{1 + t'^2}$, and since $t' > t_s$,

$$Z(t') > \xi_b \sqrt{1 + t_s^2} \geq L,$$

substituting the definition of t_s from Eq. (56). Thus the first crossing τ necessarily occurs *before* $t = t'$ and we have

$$t_s \leq \tau \leq t'. \quad (57)$$

Since t' lies within *at most* one full cycle after t_s , subtracting Eq. (40) evaluated at $t = t_s$ from that evaluated at $t = t'$ implies

$$\sinh^{-1} t' \leq \sinh^{-1} t_s + \frac{2}{\sqrt{\omega}} \int_{\xi_s}^{\xi_b} \frac{d\xi}{\sqrt{\ln(\xi^2/g) - \xi^2}}. \quad (58)$$

For any initial condition of the trajectory, the above integral remains bounded:

$$\begin{aligned} \int_{\xi_s}^{\xi_b} \frac{d\xi}{\sqrt{\ln(\xi^2/g) - \xi^2}} &\leq \int_{\xi_s}^{\xi_b} \frac{d\xi}{\sqrt{(\xi - \xi_s)(\xi_b - \xi)}} \\ &= \int_{\xi_s}^{\xi_b} \frac{d\xi}{\sqrt{\left(\frac{\xi_b - \xi_s}{2}\right)^2 - \left(\xi - \frac{\xi_b + \xi_s}{2}\right)^2}} \\ &= \int_{-1}^1 \frac{du}{\sqrt{1 - u^2}} = \pi, \end{aligned}$$

substituting $\xi = \frac{\xi_b - \xi_s}{2} u + \frac{\xi_b + \xi_s}{2}$ in the second line above. The remaining term on the right-hand side of Eq. (58) is also bounded, since $t_s \leq \sqrt{L^2 - 1}$ as a result of Eqs. (54) and (56), thus yielding

$$\tau \leq \sinh \left(\frac{2\pi}{\sqrt{\omega}} + \sinh^{-1} \sqrt{L^2 - 1} \right), \quad (59)$$

via Eq. (57). The first crossing time of *any* Bohmian trajectory is therefore bounded from above. Hence, irrespective of the initial position, the particle strikes the plane $z = L$ before a maximum arrival time τ_{\max} .

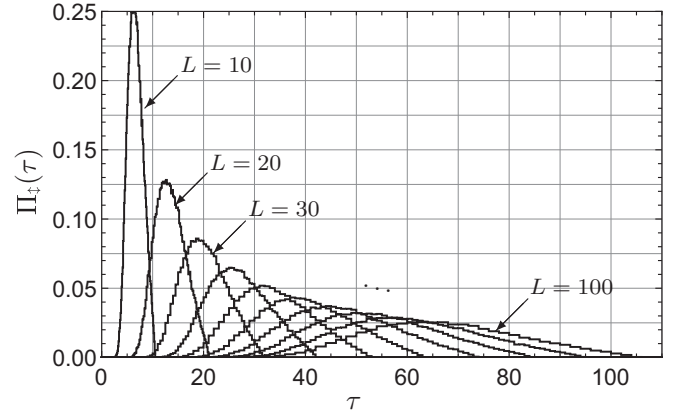


FIG. 9. Up-down arrival time histograms for select values of L and $\omega = 500$. Each histogram is constructed from $\approx 10^5$ Bohmian trajectories, whose initial conditions were sampled randomly from the initial $|\Psi|^2$ distribution (43). It should be noted that for every L there exists a maximal arrival time τ_{\max} .

To illustrate this better, we sample $N \approx 10^5$ random initial positions from the $|\Psi_0|^2$ distribution Eq. (43), solve the up-down equations of motion Eq. (21) numerically for each point in this ensemble, continuing until the trajectory hits $z = L$, then record the arrival time and plot the histogram for $\Pi_{\dagger}(\tau)$, Fig. 9. Note that a τ_{\max} occurs regardless of L . Figure 10 plots the mean $\langle \tau \rangle_{\dagger}$, standard deviation Δ_{\dagger} , and τ_{\max} of these histograms against L . Indeed, τ_{\max} lies well below the threshold permitted by Eq. (59).

C. Trapping frequency limits

The trapping frequency ω measures the effective diameter of the waveguide, which we take to be the width of the radial wave function, viz., $\sqrt{\hbar/m\omega}$ ($= 1/\sqrt{\omega}$ in our dimensionless units); typical particle trajectories also lie within this distance

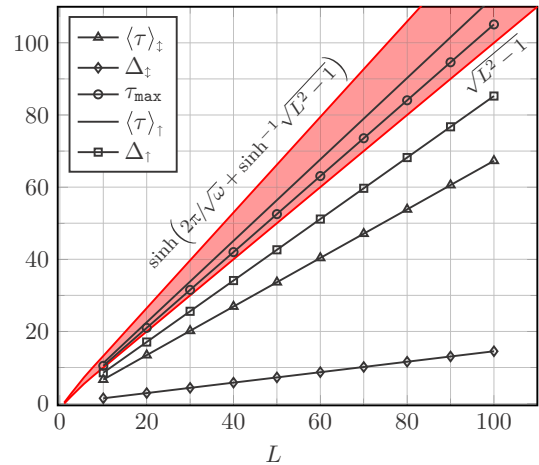


FIG. 10. Graphs of mean first arrival time $\langle \tau \rangle$ and standard deviation Δ vs L for a fixed $\omega = 500$. The spin-up statistics, unlike the up-down ones, are independent of ω . The maximum arrival time τ_{\max} of the up-down distribution is also depicted here, which lies in the shaded region permitted by inequality (59).

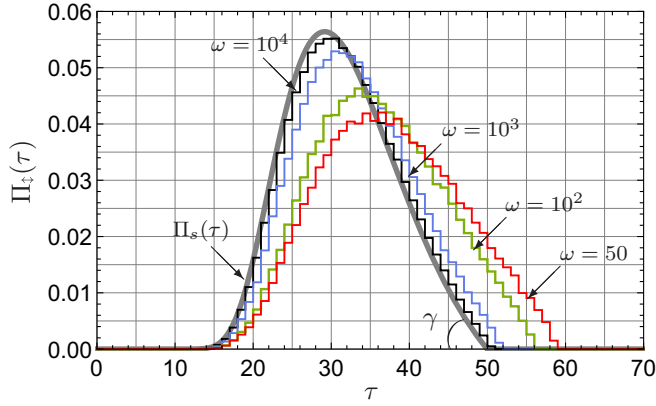


FIG. 11. Up-down arrival time histograms for select values of ω and $L = 50$. The histograms approach $\Pi_s(\tau)$, the distribution of t_s (thick gray curve), as $\omega \rightarrow \infty$, while $\tau_{\max} \rightarrow \sqrt{L^2 - 1} \approx 50$. The angle subtended at the foot of the distribution, the podal angle, $\gamma \approx \tan^{-1}(4.16/L^2)$.

from the waveguide axis. We consider here the behavior of the arrival time distributions with changing ω , for a fixed L . As noted at the end of Sec. V A, the spin-up distribution is independent of ω , so in what follows we focus on the spin-up-down distribution.

In the limit $\omega \rightarrow 0$, the radial confinement of the waveguide is absent, the distribution $\Pi_{\uparrow}(\tau)$ reduces to the spin-up distribution $\Pi_{\uparrow}(\tau)$ [Eq. (51)], while the maximum arrival time τ_{\max} is pushed to infinity. This can be seen from Eq. (21c), which for small ω approaches its spin-up analog, Eq. (20c). The latter led directly to the spin-up distribution in Sec. V A. However, in this limit, the respective Bohmian trajectories remain manifestly different: the spin-up trajectories are straight lines running parallel to the z axis, while the spin-up-down trajectories take the form $X(t) = X_0$,

$$Y(t) \approx Y_0 + \left(\frac{1}{Z_0} - Z_0 \right) \sinh^{-1} t, \quad Z(t) \approx Z_0 \sqrt{1 + t^2}.$$

On the other hand, in the limit $\omega \rightarrow \infty$, the wave function gets compressed onto the waveguide axis, effectively fusing the trajectories onto the same. Even in this rather singular limit, the up-down arrival time distribution converges to a well-defined distribution, a feature illustrated numerically in Fig. 11. This behavior can be anticipated from the combined inequality (57) and (58):

$$t_s \leq \tau \leq \sinh \left(\frac{2\pi}{\sqrt{\omega}} + \sinh^{-1} t_s \right), \quad (60)$$

which suggests that the first arrival time τ approaches t_s , as $\omega \rightarrow \infty$. However, this has to be taken cum grano salis, since t_s itself depends intricately on ω and \mathbf{R}_0 . Therefore, we consider the convergence of $\tau \rightarrow t_s$ in distribution.

From the left inequality of (60), we have

$$P(\tau \leq t) = P(t_s \leq \tau \text{ and } t_s \leq t) \leq P(t_s \leq t), \quad (61)$$

where $P(\cdot)$ is the Born probability, given by the $|\Psi_0|^2$ measure. Now, using the right inequality of (60), rewritten as

$$\sinh \left(\sinh^{-1} \tau - \frac{2\pi}{\sqrt{\omega}} \right) \leq t_s, \quad (62)$$

we have, for a given t ,

$$\begin{aligned} P \left[t_s \leq \sinh \left(\sinh^{-1} t - \frac{2\pi}{\sqrt{\omega}} \right) \right] \\ &= P \left[(62) \text{ and } t_s \leq \sinh \left(\sinh^{-1} t - \frac{2\pi}{\sqrt{\omega}} \right) \right] \\ &\leq P \left[\sinh \left(\sinh^{-1} \tau - \frac{2\pi}{\sqrt{\omega}} \right) \leq \sinh \left(\sinh^{-1} t - \frac{2\pi}{\sqrt{\omega}} \right) \right] \\ &= P(\tau \leq t). \end{aligned} \quad (63)$$

Combining the above with (61) yields

$$P \left[t_s \leq \sinh \left(\sinh^{-1} t - \frac{2\pi}{\sqrt{\omega}} \right) \right] \leq P(\tau \leq t) \leq P(t_s \leq t). \quad (64)$$

To take the limit $\omega \rightarrow \infty$ in (64), we observe that

$$P(t_s \leq t) = \int_0^t dt' \Pi_s(t'), \quad (65)$$

where Π_s is the density of t_s . As shown in Appendix B, Π_s is independent of ω , thus $P(t_s \leq t)$ is unaffected in the limit $\omega \rightarrow \infty$. As a result,

$$\lim_{\omega \rightarrow \infty} P(\tau \leq t) = \int_0^t dt' \Pi_s(t'), \quad (66)$$

and formally $\Pi_{\uparrow}(t) (:= d/dt P(\tau \leq t)) \rightarrow \Pi_s(t)$, explaining Fig. 11.

To put this result in perspective, consider a $^{40}\text{Ca}^+$ ion of mass $m \approx 6.6 \times 10^{-26}$ kg, initially trapped in the region $0 < z < \sqrt{\hbar/m\omega_z} \approx 10^{-6}$ m, or $\omega_z \approx 10^4$ rad/s, and moving in a quadrupole ion trap waveguide. The typical trapping frequencies range from $\omega \approx 10^7$ – 10^{11} rad/s, which in our dimensionless units correspond to $\omega \approx 10^3$ – 10^7 . For these specifications we will, for all practical purposes, end up with the limiting distribution Π_s , as shown in Fig. 11. An explicit formula for this distribution is therefore desirable. We perform such a calculation in Appendix B, finding

$$\Pi_s(\tau) = \frac{\tau L}{(1 + \tau^2)^{3/2}} \theta(\sqrt{L^2 - 1} - \tau) \Lambda \left(\frac{L}{\sqrt{1 + \tau^2}} \right) + \eta \delta(\tau), \quad (67)$$

where

$$\begin{aligned} \Lambda(x) &= \frac{8x}{\pi \lambda_0} (x^2 - 1) e^{-x^2} \int_{\ell(x)}^x \frac{du}{\sqrt{2 \ln(u/x) + x^2 - u^2}}, \quad (68) \\ \eta &:= \int_L^\infty dx \Lambda(x), \quad \ell(x) := \sqrt{-W_0(-x^2 e^{-x^2})}. \end{aligned} \quad (69)$$

Note that this distribution vanishes for any $\tau \geq \sqrt{L^2 - 1}$, the limiting value of τ_{\max} . A tangent line to the distribution at this point defines an angle γ with the τ axis (indicated in Fig. 11) given by

$$\gamma \approx \tan^{-1} \left(\frac{4.16}{L^2} \right), \quad L \gg 1. \quad (70)$$

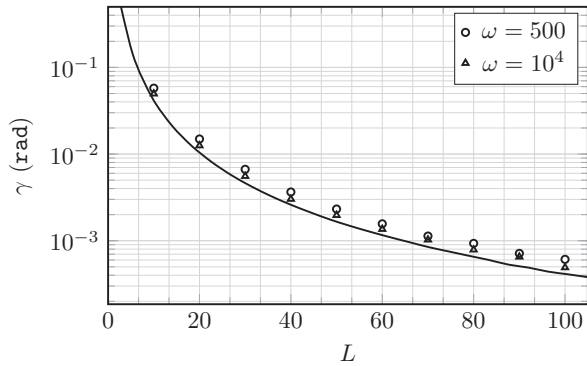


FIG. 12. Comparison of the theoretically calculated podal angle of the limiting distribution ($\omega \rightarrow \infty$) with numerical estimates for two (large) values of ω .

This *podal angle* is a notable characteristic of the up-down distribution. In Fig. 12 we plot numerical estimates of γ against L for two large values of ω , obtaining good agreement with Eq. (70).

A further surprising feature of the limiting distribution Eq. (67) is the appearance of a singular term, $\eta\delta(\tau)$, which implies that a few arrivals occur *instantaneously* in the limit $\omega \rightarrow \infty$. In practice, we cannot observe such arrivals by simply choosing a large value of ω and, more to the point, initial conditions associated with them are located very near the end face $z = 0$ of the waveguide and hence are atypical.

VI. CONCLUDING REMARKS

Our findings for the spin-up and the spin-up-down wave functions with all essential details are collected in Table I.

In comparing with results found in [28] we would like to emphasize the following: the maximum arrival time τ_{\max} reported in [28] also manifests in the model considered in this paper, and is shown here to be a consequence of certain special dynamical properties of the Bohmian trajectories, namely, (i) the natural convection of the trajectories driven by the dispersing wave packet, (ii) a quasiperiodic oscillation of the variable $\xi(t) = \frac{Z(t)}{\sqrt{1+t^2}}$, and (iii) a uniform lower bound (over all initial positions) for the maximum ξ_b [cf. Eq. (37)] of these oscillations.

The confining waveguide certainly plays a key role here, since the oscillations of ξ are suppressed in the “no waveguide” limit, $\omega \rightarrow 0$, and the up-down arrival times approach the spin-up ones. The latter satisfy only property (i).

For the model considered in [28] (cf. Fig. 2), these properties are difficult to verify, as the wave function separates into an infinite collection of tiny ripples near $z \approx d$ as soon as the barrier is switched off at $t = 0$ [29,30]. The ripples, in the course of time, develop into wave packets (separated by nodes), each propagating dispersively along the waveguide.⁵ Each of the smaller lobes of the arrival time histogram, Fig. 3, is caused by the arrival of particles propagating within

the support of *one* such wave packet. In particular, due to the nodes separating these wave packets, the particle remains within the support of the *particular* wave packet for which its random initial position was realized at $t = 0^+$. The nodes move forward in time, carrying the particle along; hence the arrival times are recorded in bunches.

The Bohmian dynamics within a given wave packet is very similar to the Bohmian dynamics of the waveguide-confined particle studied here, in the sense that the rear node of a given wave packet resembles the waveguide hard wall at $z = 0$, while the frontal node is analogous to the vanishing tail of the wave function Eq. (15). Continuing the analogy, the results of this paper would suggest the appearance of a “maximum arrival time” for each wave packet. Such a τ_{\max} would necessarily be smaller than the time at which the rear node of the preceding wave packet crossed L . This is consistent with the formation of “no arrival windows” found numerically in [28] and illustrated in Fig. 3.

Questions not addressed in this paper concern the experimental relevance of the first arrival times of Bohmian trajectories. We mentioned previously the problem of backscattering of the detector on the wave function, which may be modeled by an imaginary potential barrier [18]. Another project underway is the study of relativistic corrections to the results of [28], using the Bohm-Dirac guidance law. Finally, experimental realizations of the waveguide and detector (e.g., [23] or [41]) are currently being discussed.

ACKNOWLEDGMENTS

We thank J. M. Wilkes for critically reviewing our manuscript and suggesting numerous edits, which improved the paper significantly. We thank Dustin Lazarovici and Matthias Lienert for a careful reading of a preliminary version of our paper. Thanks are also due to Dipankar Home and Peter R. Holland for helpful discussions. M.N. acknowledges funding from the Elite Network of Bavaria, through the Junior Research Group “Interaction Between Light and Matter”.

APPENDIX A: TIME EVOLUTION OF Ψ_0

The Pauli equation (8) with initial condition (11) can be solved as follows: applying the identity $(\boldsymbol{\sigma} \cdot \nabla)^2 = \nabla^2 \mathbb{1}$ (where $\mathbb{1}$ is the 2×2 unit matrix), the right-hand side of Eq. (8) becomes diagonal, essentially simplifying it to the Schrödinger equation

$$i \frac{\partial \psi_t}{\partial t} = -\frac{1}{2} \nabla^2 \psi_t + \left[\frac{\omega^2}{2} (x^2 + y^2) + v(z) \right] \psi_t, \quad (\text{A1})$$

for the spatial part of the spinor wave function Ψ , with initial condition (12). The constant spinor forming the spin part of the wave function remains unchanged. Now, employing the ansatz

$$\psi_t(\mathbf{r}) = \varphi_t(z) e^{-\frac{\omega}{2}(x^2+y^2) - i\omega t} \quad (\text{A2})$$

⁵This remarkable wave phenomenon, known as *diffraction in time* [40], manifests in response to a sudden change in the boundary conditions of the wave function at a given surface (in this case,

the plane $z = d$). For the harmonic barrier $\frac{1}{2}m\omega_z^2 z^2$ considered in this paper, such conditions are not met; consequently no ripples are observed.

in Eq. (A1), we arrive at the PDE

$$i \frac{\partial \varphi_t}{\partial t} = -\frac{1}{2} \frac{\partial^2 \varphi_t}{\partial z^2} + v(z) \varphi_t, \quad (\text{A3})$$

for the function φ_t , which satisfies $\varphi_0(z) = A \theta(z) z e^{-\frac{z}{2}}$. Equation (A3) is simply the one-dimensional Schrödinger equation for a particle subject to a hard-wall potential barrier at $z = 0$; thus $\varphi_t(z) = 0$ for any $z \leq 0$. In the region $z > 0$, the solution of Eq. (A3) can be written as

$$\varphi_t(z) = \int_0^\infty dz' K(z, t | z', 0) \varphi_0(z'), \quad (\text{A4})$$

where

$$K(z, t | z', 0) = \frac{e^{\frac{i}{2t}(z-z')^2}}{\sqrt{2\pi it}} - \frac{e^{\frac{i}{2t}(z+z')^2}}{\sqrt{2\pi it}} \quad (\text{A5})$$

is the propagator (or Green's function) of Eq. (A3) [42]. Exploiting the symmetry of the integrand in Eq. (A4) to extend the integral to $-\infty < z' < \infty$ allows writing the solution as

$$\begin{aligned} \varphi_t(z) &= \frac{A}{2\sqrt{2\pi it}} \int_{-\infty}^\infty dz' z' \left[\exp\left(\frac{i}{2t}(z-z')^2 - \frac{z'}{2}\right) \right. \\ &\quad \left. - \exp\left(\frac{i}{2t}(z+z')^2 - \frac{z'}{2}\right) \right] \\ &= \frac{A e^{iz^2/2t}}{\sqrt{2\pi it}} \int_{-\infty}^\infty dz' z' (-i) \sin\left(\frac{zz'}{t}\right) e^{-\left(\frac{1}{2} - \frac{i}{2t}\right)z'} \\ &= \frac{A e^{iz^2/2t}}{\sqrt{2\pi it}} \int_{-\infty}^\infty dz' z' \exp\left[-\left(\frac{1}{2} - \frac{i}{2t}\right)z'^2 - \frac{iz}{t}z'\right] \\ &= \frac{Az}{(1+it)^{3/2}} e^{-\frac{z^2}{2(1+it)}} \end{aligned} \quad (\text{A6})$$

using the identity

$$\frac{2}{\sqrt{\pi}} \int_{-\infty}^\infty dx x e^{-ax^2+bx} = \frac{b}{a^{3/2}} e^{b^2/4a}, \quad \text{Re}[a] > 0. \quad (\text{A7})$$

The final solution thus reduces to (16).

APPENDIX B: DISTRIBUTION OF t_s

Equation (56) expresses t_s as a function of ξ_b , which takes values in the interval $[1, \infty)$ [see Eq. (54)]. Thus the distribution of t_s may be written as

$$\Pi_s(t) = \int_1^\infty d\xi_b \delta(t_s(\xi_b) - t) \Lambda(\xi_b), \quad (\text{B1})$$

where Λ is the distribution of ξ_b , given by

$$\Lambda(\xi_b) = 1/\lambda_0 \int_{0 < Z_0 < L} d^3 \mathbf{R}_0 \delta(\xi_b(Y_0, Z_0) - \xi_b) |\Psi_0|^2(\mathbf{R}_0). \quad (\text{B2})$$

Here, $\xi_b(Y_0, Z_0)$ is defined via Eqs. (37) and (32):

$$\xi_b(Y_0, Z_0) \equiv \xi_b(g(Y_0, Z_0)) = \sqrt{-W_{-1}(-Z_0^2 e^{-Z_0^2 - \omega Y_0^2})}. \quad (\text{B3})$$

Substituting the definition of t_s , Eq. (56) in Eq. (B1), we obtain

$$\begin{aligned} \Pi_s(t) &= \int_1^L d\xi_b \delta\left(\sqrt{\frac{L^2}{\xi_b^2} - 1} - t\right) \Lambda(\xi_b) \\ &\quad + \delta(t) \int_L^\infty d\xi_b \Lambda(\xi_b). \end{aligned} \quad (\text{B4})$$

We shall denote the integral multiplying $\delta(t)$ by

$$\eta := \int_L^\infty d\xi_b \Lambda(\xi_b). \quad (\text{B5})$$

The remaining integral in Eq. (B4) can be evaluated with the help of identity (47), exactly as in Sec. V A, with the final result

$$\Pi_s(t) = \frac{tL}{(1+t^2)^{3/2}} \theta(\sqrt{L^2-1}-t) \Lambda\left(\frac{L}{\sqrt{1+t^2}}\right) + \eta \delta(t). \quad (\text{B6})$$

Note that $\Pi_s(t)$ vanishes for any $t > \sqrt{L^2-1}$, regardless of the specific form of $\Lambda(\xi_b)$.

Next, we turn to the evaluation of $\Lambda(\xi_b)$. Substituting $|\Psi_0|^2(\mathbf{R}_0)$ [Eq. (43)] in Eq. (B2), and integrating over X_0 , yields

$$\begin{aligned} \Lambda(\xi_b) &= \frac{4\sqrt{\omega}}{\pi \lambda_0} \int_0^L dZ_0 Z_0^2 \int_{-\infty}^\infty dY_0 \\ &\quad \times \delta(\xi_b(Y_0, Z_0) - \xi_b) e^{-Z_0^2 - \omega Y_0^2}. \end{aligned} \quad (\text{B7})$$

Once again, recalling identity (47), with

$$\phi(Y_0) = \xi_b(Y_0, Z_0) - \xi_b, \quad (\text{B8})$$

we compute the zeros of ϕ , satisfying $\xi_b(Y_0, Z_0) = \xi_b$,

$$\begin{aligned} &\Rightarrow W_{-1}(-Z_0^2 e^{-Z_0^2 - \omega Y_0^2}) = -\xi_b^2 \\ &\Rightarrow e^{-\omega Y_0^2} = \frac{\xi_b^2 e^{-\xi_b^2}}{Z_0^2 e^{-Z_0^2}} \end{aligned} \quad (\text{B9})$$

$$\Rightarrow Y_0 = \pm \sqrt{\frac{2 \ln(Z_0/\xi_b) + \xi_b^2 - Z_0^2}{\omega}} \equiv Y_{0\pm}. \quad (\text{B10})$$

In Eq. (B9), we invoked the defining property of the Lambert W function: $W(a) = b \Leftrightarrow a = be^b$ [39]. We evaluate $\phi'(Y_{0\pm})$ as follows:

$$\begin{aligned} \phi'(Y_{0\pm}) &= \frac{\partial \xi_b(Y_0, Z_0)}{\partial Y_0} \Big|_{Y_{0\pm}} = \frac{\partial \xi_b(g)}{\partial g} \frac{\partial g}{\partial Y_0} \Big|_{Y_{0\pm}} \\ &= \frac{-W_{-1}(g)}{2g\xi_b(g)[1+W_{-1}(g)]} (-2g\omega Y_0) \Big|_{Y_{0\pm}} \\ &= \omega Y_{0\pm} \frac{\xi_b}{\xi_b^2 - 1}. \end{aligned} \quad (\text{B11})$$

Here, we used the identity $W' = W/z(1+W)$ [39]. Putting all the pieces together yields

$$\begin{aligned} \delta(\xi_b(Y_0, Z_0) - \xi_b) &= \theta(Z_0^2 e^{-Z_0^2} - \xi_b^2 e^{-\xi_b^2}) \frac{\xi_b^2 - 1}{\omega \xi_b Y_{0+}} \\ &\quad \times [\delta(Y_0 - Y_{0+}) + \delta(Y_0 - Y_{0-})] \end{aligned} \quad (\text{B12})$$

via (47). Note that the Heaviside function $\theta(\cdot)$ eliminates any Z_0 that gives rise to an imaginary $Y_{0\pm}$, which therefore does

not contribute to the integral (B7). Substituting Eq. (B12) into Eq. (B7) and evaluating the integral over Y_0 yields

$$\begin{aligned}\Lambda(\xi_b) &= \frac{8(\xi_b^2 - 1)}{\pi \lambda_0 \xi_b \sqrt{\omega}} \int_0^L dZ_0 \frac{Z_0^2}{Y_{0+}^2} \theta(Z_0^2 e^{-Z_0^2} - \xi_b^2 e^{-\xi_b^2}) e^{-Z_0^2 - \omega Y_{0+}^2} \\ &= \frac{8\xi_b}{\pi \lambda_0} (\xi_b^2 - 1) e^{-\xi_b^2} \int_0^L dZ_0 \frac{\theta(Z_0^2 e^{-Z_0^2} - \xi_b^2 e^{-\xi_b^2})}{\sqrt{2 \ln(Z_0/\xi_b) + \xi_b^2 - Z_0^2}},\end{aligned}\quad (\text{B13})$$

using Eqs. (B9) and (B10). Note that ω dropped out obligingly in the previous step. Now, for a given $\xi_b \geq 1$, the inequality $Z_0^2 e^{-Z_0^2} > \xi_b^2 e^{-\xi_b^2}$ implies

$$\underbrace{\sqrt{-W_0(-\xi_b^2 e^{-\xi_b^2})}}_{=: \ell(\xi_b)} < Z_0 < \underbrace{\sqrt{-W_{-1}(-\xi_b^2 e^{-\xi_b^2})}}_{=: \xi_b},$$

which, incorporated into Eq. (B13), yields the final result

$$\Lambda(\xi_b) = \frac{8\xi_b}{\pi \lambda_0} (\xi_b^2 - 1) e^{-\xi_b^2} \int_{\ell(\xi_b)}^{\min\{\xi_b, L\}} \frac{dZ_0}{\sqrt{2 \ln(Z_0/\xi_b) + \xi_b^2 - Z_0^2}}.\quad (\text{B14})$$

Since we evaluate $\Lambda(\cdot)$ at $L/\sqrt{1+t^2}$ in Eq. (B6), the upper limit of the integral can be simply replaced by ξ_b .

-
- [1] G. R. Allcock, *Ann. Phys. (NY)* **53**, 253 (1969).
[2] G. R. Allcock, *Ann. Phys. (NY)* **53**, 286 (1969).
[3] Y. Aharonov and D. Bohm, *Phys. Rev.* **122**, 1649 (1961).
[4] *Time in Quantum Mechanics*, edited by J. G. Muga, R. S. Mayato, and Í. L. Egusquiza, Lecture Notes in Physics No. 734, 2nd ed. (Springer, Berlin Heidelberg, 2008), Vol. 1.
[5] J. G. Muga and C. R. Leavens, *Phys. Rep.* **338**, 353 (2000).
[6] *The Message of Quantum Science: Attempts Towards a Synthesis*, edited by P. Blanchard and J. Fröhlich, Lecture Notes in Physics No. 899 (Springer, Berlin Heidelberg, 2015).
[7] C. R. Leavens, *Phys. Lett. A* **303**, 154 (2002).
[8] B. Mielnik and G. Torres-Vega, *Universal J. Phys. Appl.* **II**, 81 (2005).
[9] E. A. Galapon, R. F. Caballar, and R. T. Bahague Jr., *Phys. Rev. Lett.* **93**, 180406 (2004).
[10] D. Dürr, S. Goldstein, and N. Zanghì, *J. Stat. Phys.* **116**, 959 (2004).
[11] J. Kijowski, *Rep. Math. Phys.* **6**, 361 (1974).
[12] R. Werner, *J. Math. Phys.* **27**, 793 (1986).
[13] C. Anastopoulos and N. Savvidou, *J. Math. Phys.* **47**, 122106 (2006).
[14] R. Tumulka, [arXiv:1601.03715](https://arxiv.org/abs/1601.03715).
[15] T. Zimmermann, S. Mishra, B. R. Doran, D. F. Gordon, and A. S. Landsman, *Phys. Rev. Lett.* **116**, 233603 (2016).
[16] N. Douguet and K. Bartschat, *Phys. Rev. A* **97**, 013402 (2018).
[17] S. Kocsis *et al.*, *Science* **332**, 1170 (2011).
[18] S. Das, M. Nöth, and D. Dürr (unpublished).
[19] L. Kellers, Master's thesis, LMU Munich & TU Munich, 2017, www.mathematik.uni-muenchen.de/~7Ebohmmech/theses/Kellers_Leopold_MA.pdf.
[20] T. Hils, J. Felber, R. Gähler, W. Gläser, R. Golub, K. Habicht, and P. Wille, *Phys. Rev. A* **58**, 4784 (1998).
[21] Y. Uehara *et al.*, *Jpn. J. Appl. Phys.* **29**, 2858 (1990).
[22] A. Kothe *et al.*, *Rev. Sci. Instrum.* **84**, 023106 (2013).
[23] K. Groot-Berning *et al.*, *Phys. Rev. A* **99**, 023420 (2019).
[24] P. Szriftgiser, D. Guéry-Odelin, M. Arndt, and J. Dalibard, *Phys. Rev. Lett.* **77**, 4 (1996).
[25] C. Salomon, J. Dalibard, W. D. Phillips, A. Clairon, and S. Guellati, *EPL* **12**, 683 (1990).
[26] A. Fuhrmanek, A. M. Lance, C. Tuchendler, P. Grangier, Y. R. P. Sortais, and A. Browaeys, *New J. Phys.* **12**, 053028 (2010).
[27] F. Delgado, J. G. Muga, and G. García-Calderón, *Phys. Rev. A* **74**, 062102 (2006).
[28] S. Das and D. Dürr, *Sci. Rep.* **9**, 2242 (2019).
[29] S. Das, Master's thesis, LMU Munich & TU Munich, 2017, http://www.mathematik.uni-muenchen.de/~bohmmech/theses/Das_Siddhant_MA.pdf.
[30] S. Das and D. Dürr (unpublished).
[31] P. R. Holland and C. Philippidis, *Phys. Rev. A* **67**, 062105 (2003).
[32] D. Bohm and B. J. Hiley, *The Undivided Universe: An Ontological Interpretation of Quantum Theory* (Routledge, London and New York, 1993).
[33] K. Berndl, D. Dürr, S. Goldstein, G. Peruzzi, and N. Zanghì, *Commun. Math. Phys.* **173**, 647 (1995).
[34] S. Teufel and R. Tumulka, *Commun. Math. Phys.* **258**, 349 (2005).
[35] J. J. Sakurai and J. Napolitano, *Modern Quantum Mechanics*, 2nd ed. (Addison-Wesley, San Francisco, 1994).
[36] P. R. Holland, *Ann. Phys. (Leipzig)* **12**, 446 (2003).
[37] P. R. Holland, *Phys. Rev. A* **60**, 4326 (1999).
[38] D. Dürr, S. Goldstein, and N. Zanghì, *J. Stat. Phys.* **67**, 843 (1992).
[39] R. M. Corless, G. H. Gonnet, D. E. G. Hare, D. J. Jeffrey, and D. E. Knuth, *Adv. Comput. Math.* **5**, 329 (1996).
[40] M. Moshinsky, *Phys. Rev.* **88**, 625 (1952).
[41] J. A. Damborenea, I. L. Egusquiza, G. C. Hegerfeldt, and J. G. Muga, *Phys. Rev. A* **66**, 052104 (2002).
[42] M. Goodman, *Am. J. Phys.* **49**, 843 (1981).